Editors' Suggestion

Low-energy interband transition in the infrared response of the correlated metal $SrVO_3$ in the ultraclean limit

Gihyeon Ahn,[1] M. Zingl,[2] S. J. Noh,[1] M. Brahlek,[3] Joseph D. Roth,[3] Roman Engel-Herbert,[3,4,5] A. J. Millis,[2,6] and S. J. Moon[1,*]

[1]*Department of Physics, Hanyang University, Seoul 04763, Republic of Korea*
[2]*Center for Computational Quantum Physics, Flatiron Institute, 162 5th Avenue, New York, New York 10010, USA*
[3]*Department of Materials Science and Engineering, Pennsylvania State University, University Park, Pennsylvania 16802, USA*
[4]*Department of Physics, Pennsylvania State University, University Park, Pennsylvania 16802, USA*
[5]*Department of Chemistry, Pennsylvania State University, University Park, Pennsylvania 16802, USA*
[6]*Department of Physics, Columbia University, New York, New York 10027, USA*

(Received 2 June 2022; accepted 4 August 2022; published 24 August 2022)

We studied the low-energy electronic response of the prototypical correlated metal $SrVO_3$ in the ultraclean and disordered limit using infrared spectroscopy and density functional theory plus dynamical mean field theory calculations (DFT + DMFT). A strong optical excitation at 70 meV is observed in the optical response of the ultraclean samples but is hidden by the low-energy Drude-like response from intraband excitations in the more disordered samples. DFT + DMFT calculations reveal that this optical excitation originates from interband transitions between the bands split by orbital off-diagonal hopping, which has often been ignored in cubic systems, such as $SrVO_3$. A memory function analysis of the optical data shows that this interband transition can lead to deviations of optical self-energy from the expected Fermi-liquid behavior. Our findings demonstrate that analysis schemes employed to extract many-body effects from optical spectra may be oversimplified to study the true electronic ground state and that improvements in material quality can guide efforts to refine theoretical approaches.

DOI: 10.1103/PhysRevB.106.085133

I. INTRODUCTION

Fermi-liquid theory is a cornerstone of the current understanding of the metallic state of condensed matter [1]. The characteristic feature of a Fermi liquid is the presence of well-defined quasiparticles with a scattering rate that is smaller than their energy ($\hbar\omega$) and temperature (T), and varies as ω^2 and T^2. The responses of some correlated metals deviate from the responses expected in Fermi-liquid theory. Prominent examples include the linear increase in the resistivity with T without a saturation, while the Fermi-liquid T^2 behavior appears at very low temperatures. This strange metallic behavior is one of the most enigmatic problems in condensed matter physics [2–4].

Optical spectroscopy has played a pivotal role in documenting the strange metallic behavior of the low-energy electronic response of strongly correlated electron systems [5–7]. Optical signatures of the non-Fermi liquid include a slower decay of the real part of the optical conductivity $\sigma_1(\omega)$ than ω^{-2} expected for the Drude response, and sizeable spectral weight at midinfrared energies of $\hbar\omega \geqslant 0.1$ eV [8–13]. Dynamical mean field theory (DMFT) studies suggested that well-defined quasiparticles survive in a broad temperature range [14–16], and these "resilient" quasiparticles are responsible for the large midinfrared conductivity [14,17]. The scattering rate of the resilient quasiparticles are expected to show a saturation or decrease at finite frequencies, and thus the quasiparticles have larger velocities above the corresponding energies than the bare velocity from the band dispersion, leading to an excess spectral weight in $\sigma_1(\omega)$ [14,17]. The picture of the resilient quasiparticles is applied to describe optical experiments on correlated metallic ruthenates, vanadates, and the nickelates [16,18,19].

In multiband systems, band structure effects can complicate the low-energy optical response. Structural distortions in multiband metal can induce interband transitions. It was shown that the $GdFeO_3$-type lattice distortion in $CaRuO_3$ led to the formation of a complex Fermi surface composed of multiple pockets [20]. A density functional theory (DFT) + DMFT study on $CaRuO_3$ suggested that interband transition between bands split by the $GdFeO_3$-type orthorhombic distortions gives rise to a power-law behavior $\sigma_1(\omega) \sim \omega^{0.5}$ for frequencies below 0.1 eV [21], mimicking the non-Fermi-liquid behavior. The spin-orbit coupling can also affect the low-energy electronic response. In $\sigma_1(\omega)$ of Sr_2RhO_4, interband transitions between the spin-orbit-split bands are observed at about 0.18 eV [22]. It should be noted that the energy of this interband transition is similar with those where the excess spectral weight attributed to the resilient quasiparticle excitations are observed in Sr_2RuO_4. The complexity in the optical data of correlated metals demonstrates the importance of disentangling the effects from the band structure and electronic correlations to

*soonjmoon@hanyang.ac.kr

understand the quasiparticle dynamics in strongly correlated systems.

In this work, we investigated the electronic response of $SrVO_3$ thin films by using infrared spectroscopy and DFT + DMFT calculations. $SrVO_3$ is an archetypal correlated metal where electronic correlations are not strong enough to destabilize the metallic ground state, but play a crucial role in transport and optical properties [23–25]. Because of the cubic crystal structure [26] and the small spin-orbit coupling (∼20 meV) [27,28], it is expected that additional complexity in the optical response due to band structure effects is small. Indeed the Fermi surface and the low-energy electronic band dispersion of $SrVO_3$ can be described by the three t_{2g} orbitals with moderate bandwidth renormalization [28–33]. We also stress that our $SrVO_3$ thin film is very clean: the residual resistivity ratio (RRR) is about 130. The low disorder of the films studied enabled us to probe fine structures of the low-energy spectrum. At low temperatures, we observed an extremely narrow Drude-like peak at zero frequency and a well-defined peak structure at about 70 meV in $\sigma_1(\omega)$ of the SVO film with RRR = 130. The 70-meV structure was not resolved in $\sigma_1(\omega)$ of SVO films, with a much lower RRR = 6. We present theoretical calculations that reveal that the optical excitation at about 70 meV originates from interband transition, which is induced by an orbital off-diagonal hopping term between V sites separated at a larger than nearest-neighbor distance, and we show that in the more disordered sample, this feature appears as a non-Fermi-liquid signature in the conductivity. The intrinsic optical response of $SrVO_3$ in an ultraclean limit revealed in our work demonstrates that interband transition, which has often been neglected, can give rise to a significant contribution to an optical response even in a simple cubic system, and that the effects of interband transitions should be accounted for to understand the intrinsic electrodynamic response of correlated electron materials.

II. METHODS

A. Experiments

$SrVO_3$ thin films were grown by hybrid molecular beam epitaxy [34] on the $(LaAlO_3)_{0.3}(Sr_2TaAlO_6)_{0.7}$ (LSAT) substrate by cosupplying elemental Sr from an effusion cell and the metal–organic precursor vanadium oxytriisopropoxide (VTIP) [35]. Properly matching the Sr-to-VTIP flux ratio resulted in the growth of stoichiometric $SrVO_3$ films, which were confirmed by extracting the intrinsic lattice parameter of strained $SrVO_3$ on LSAT, resulting in an out-of-plane lattice parameter of 3.824 Å when coherently strained on LSAT, and a large RRR of over 100. High-resolution x-ray diffraction (XRD) 2θ-ω scans around the 002 peaks of LSAT and $SrVO_3$ were taken using a Phillips PANalytical X'Pert Pro using Cu-Kα_1 radiation. Thickness and intrinsic lattice parameters were extracted from the periodicity of the Kiessig fringes and the $SrVO_3$ 002 peak position. Temperature-dependent resistivity measurements using the Van der Pauw geometry and indium contacts were performed using a Quantum Design Physical Properties Measurement System operated in AC mode. The reflectivity spectra $R(\omega)$ of the $SrVO_3$/LSAT samples and the LSAT substrate between 5 meV and 1 eV

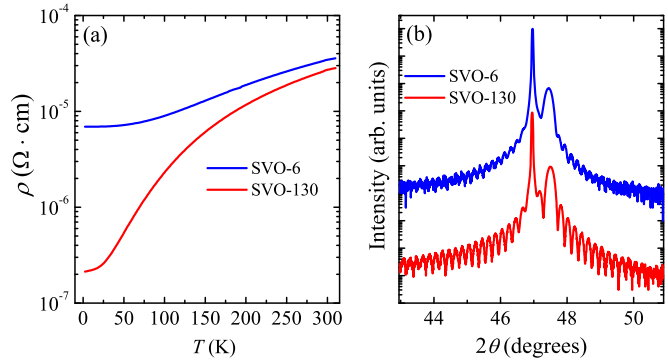

FIG. 1. (a) Temperature-dependent dc resistivity $\rho(T)$ of $SrVO_3$ films. (b) X-ray diffraction 2θ-ω scans taken around the 002 peaks of $SrVO_3$ films and LSAT substrate.

were measured using a Fourier transform infrared spectrometer (Bruker Vertex 70v) with an *in situ* overcoating technique [36]. Complex optical conductivity spectra $\sigma(\omega) = \sigma_1(\omega) + i\sigma_2(\omega)$ of the films were obtained via a two-layer model fit with Kramers–Kronig-constrained variational dielectric functions [37,38]. The optical constants in the energy region between 0.74 and 6 eV were obtained by using a spectroscopic ellipsometer.

B. Theoretical calculations

The DFT calculations were carried out by using WIEN2k [42] with the standard Perdew-Burke-Ernzerhof (PBE) version of the generalized gradient approximations (GGA) functional [43]. For the DMFT calculations, we used TRIQS/DFTTools [44] and the TRIQS/cthyb solver [45], which are based on the TRIQS library [46]. For Wannier model calculations, wien2wannier [47] and Wannier90 [48] were used to construct maximally localized Wannier functions [49,50] for the three orbitals of the t_{2g} symmetry near the Fermi energy on a $10 \times 10 \times 10$ k-point grid. Details of the calculations are described in the Supplemental Material [38].

III. RESULTS AND DISCUSSION

Figure 1 shows the resistivity and the XRD data of the $SrVO_3$ for two samples: one ultraclean (RRR = 130) and one more disordered (RRR = 6). The resistivity ρ of the two samples show metallic behavior, i.e., $d\rho/dT > 0$ at all temperatures. The RRR value, which is a measure of the sample purity, of the $SrVO_3$ film grown inside the self-regulated growth window is about 130 (SVO-130), much higher than conventional thin film and even bulk single crystals, which exhibit RRR values ranging from 2 to 56 [24,51–55]. We refer to the RRR = 130 film as the ultraclean limit. To contrast the intrinsic low-energy electronic response of ultraclean $SrVO_3$, a film with much lower RRR = 6 (SVO-6) was grown, which is similar to the crystalline quality commonly achieved. The XRD data with clear Kiessig fringes in Fig. 1(b) highlight the structural excellence of the $SrVO_3$ films. $SrVO_3$ single crystals have a cubic perovskite structure with the lattice constant $a = 3.842$ Å. Because the lattice constant of the LSAT substrate is 3.868 Å, $SrVO_3$ films are under tensile strain giving rise to an out-of-plane lattice constant of 3.824 Å for

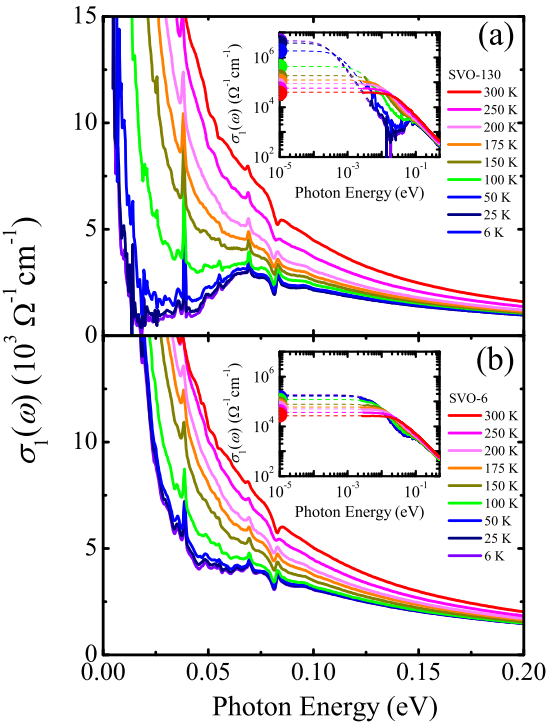

FIG. 2. The real part of optical conductivity $\sigma_1(\omega)$ for (a) $SrVO_3$ films with RRR = 130 and (b) RRR = 6. Insets: the log-log plot of $\sigma_1(\omega)$; closed circles correspond to the values of the dc conductivities taken from the $\rho(T)$ in Fig. 1. The dashed lines represent the extrapolated $\sigma_1(\omega)$.

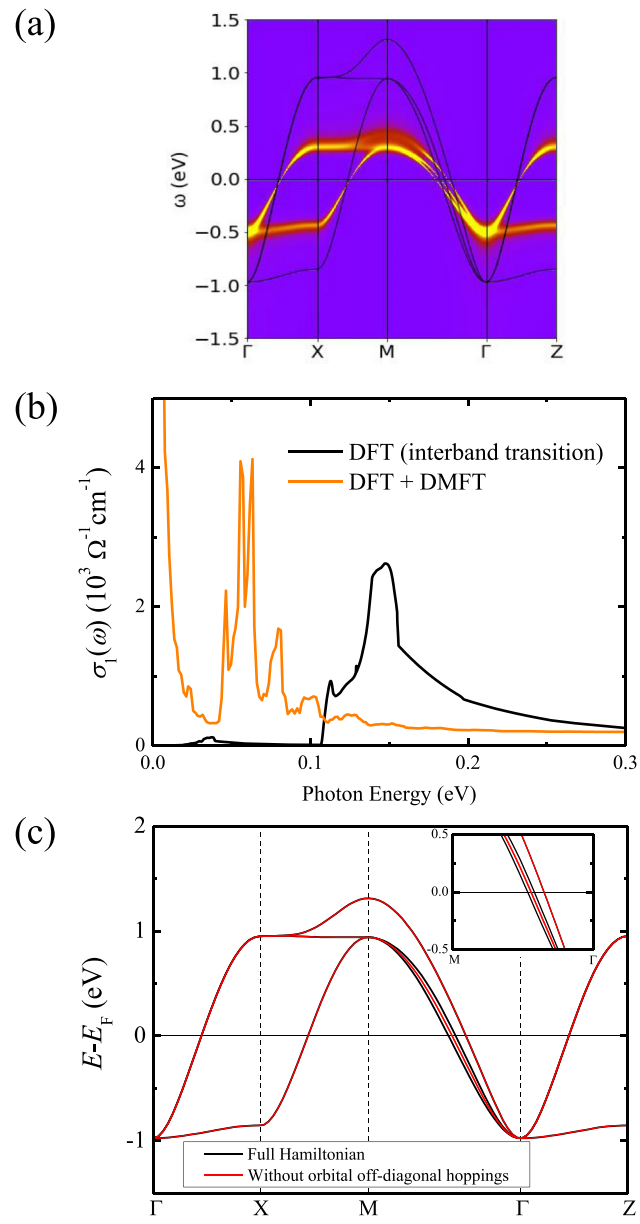

FIG. 3. (a) Band structure of $SrVO_3$ from the DFT calculations (solid line) and the spectral function from the DFT + DMFT calculations (color-coded). (b) Optical conductivity extracted from the DFT band structure (black line) and the DFT + DMFT calculations (orange line). (c) Wannier model band structures for the full Hamiltonian (black line) and without the orbital off-diagonal hopping (red line). Inset shows the zoomed-in band dispersion in the Γ-*M* direction.

stoichiometric films, and larger values in case of Sr-rich or V-rich films.

Figure 2 shows the low-energy $\sigma_1(\omega)$ of the SVO-130 and the SVO-6 films. The low-energy conductivity spectra of both the samples display a strong Drude-like peak centered at zero frequency, confirming the metallicity of the samples. The sharp peaks at about 0.038 and 0.069 eV are due to optical phonons. Insets display low-energy extrapolation of $\sigma_1(\omega)$ at different temperatures and corresponding dc conductivity values from four-probe resistivity measurements shown in Fig. 1, which are found to be in excellent agreement with the values of $\sigma_1(\omega)$ at the zero-frequency limit.

While both the samples show a metallic response, the different degree of defects present in the films gives rise to a striking difference in the spectral shape of the optical conductivity at low temperatures. The Drude-like peak in $\sigma_1(\omega)$ of the SVO-130 sample at 6 K is found to be extremely narrow, with a width of about 0.24 meV. For comparison, the width of the Drude-like peak of the SVO-6 sample at 6 K is about 5.27 meV. Due to the remarkably sharp Drude-like response, a peak structure located at about 0.07 eV is clearly resolved at low temperature in the SVO-130 sample [Fig. 2(a)]. We stress that the low-energy peak structure has not been reported in previous optical studies of $SrVO_3$ [25], which was likely masked by disorder and a resulting wider Drude-like peak. Indeed for the disordered SVO-6 sample, the peak structure is masked by a broad Drude-like response even at the lowest temperature. As the temperature increases, the peak structure in $\sigma_1(\omega)$ of the SVO-130 sample blends into the Drude-like peak due to the broadening of the latter. At 300 K, the width of the Drude-like peak of the SVO-130 sample is found to be about 30 meV, which is smaller than that of the SVO-6 sample (40 meV). With the exception of the quantitative difference in the magnitude of the conductivity, the overall spectral shapes of the room-temperature $\sigma_1(\omega)$ of the two samples are similar to each other.

The spectral shape of the low-temperature $\sigma_1(\omega)$ data of SVO-6 in Fig. 2(b), represented by a smooth midinfrared

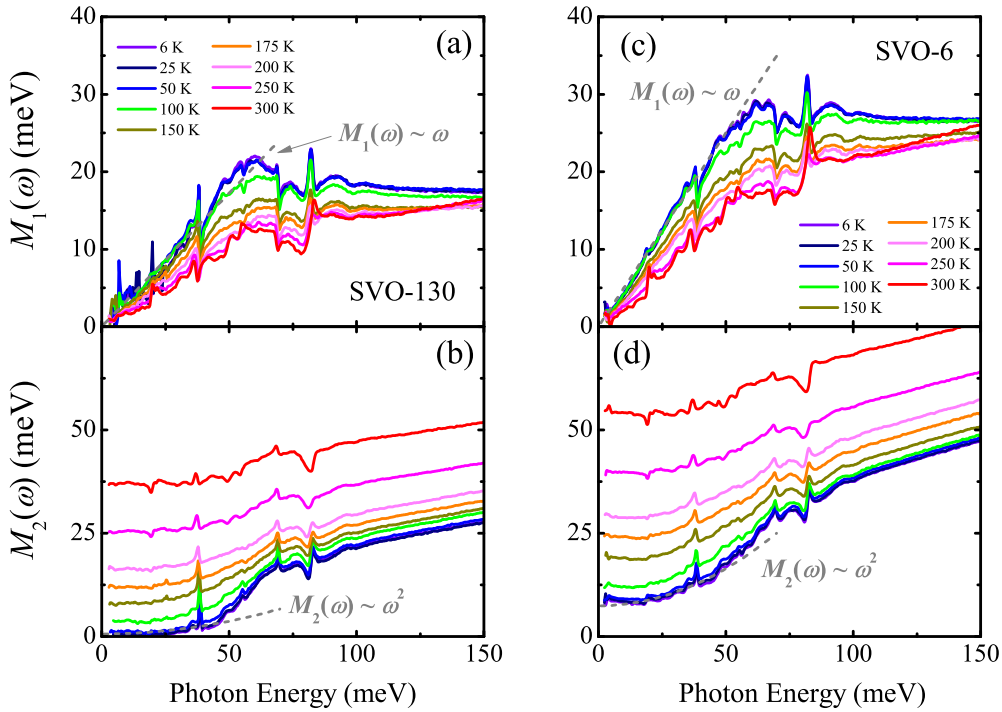

FIG. 4. (a) Real and (b) imaginary parts of the memory function of the $SrVO_3$ film with RRR = 130. (c) Real and (d) imaginary parts of the memory function of the $SrVO_3$ film with RRR = 6. Dashed lines in (a), (c) and (b), (d) represent the linear and the quadratic frequency dependences of the real and imaginary parts of the memory function at 6 K, respectively.

continuum following the Drude-like peak, is commonly observed in many strongly correlated metals [5,6,9,10]. The featureless midinfrared background has been attributed to many-body effects present in the material, such as electron–boson interactions and/or electron–electron interactions [5]. The interactions can induce a spectral weight transfer from the zero-frequency Drude-like peak into finite-energy excitations with an energy scale determined by the many-body interactions present. Such a spectral weight shift leads to the development of the smooth continuum in $\sigma_1(\omega)$; however, attributing the midinfrared continuum feature to many-body effects is based on the assumption that intraband excitations from itinerant carriers are sole contributors to the low-energy conductivity. The conductivity data of the SVO-130 sample, exhibiting the clear separation between the Drude-like response and the peak structure at about 0.07 eV, put this assumption to the test theoretically.

In order to gain insights into the origin of the low-energy peak structure in our optical data, DFT calculations were performed. Since the tetragonal distortion arising from epitaxial strain in films has been found to have only a negligible effect on band dispersion [38], which has been experimentally verified by angle-resolved photoemission spectroscopy studies of strained $SrVO_3$ films [30–32,56], we used the cubic structure of bulk $SrVO_3$. The band dispersion from the DFT calculations [black solid lines in Fig. 3(a)] between –1.5 and 1.5 eV, where the three V 3*d* t_{2g} states are main contributors, is shown in Fig. 3(a). The result is consistent with the band dispersion of the previous DFT studies of $SrVO_3$ [32,33,57,58]. The interband part of the calculated $\sigma_1(\omega)$ based on the DFT band structure predicts strong optical excitations at about 0.15 eV, as shown in Fig. 3(b). The position of the interband transition in the DFT $\sigma_1(\omega)$ is close to the 0.07 eV peak observed in the RRR = 130 sample.

A crucial aspect of the band structure is a weak splitting of the three t_{2g}-derived bands along the Γ-*M* direction. The low-energy electronic structure of $SrVO_3$ is described by the three t_{2g} orbitals [28–33]. For cubic structures, nearest-neighbor hopping is allowed only between the same orbitals (orbital-diagonal hopping) due to their symmetries, and interband transition is not allowed. The presence of the low-energy interband transitions in $\sigma_1(\omega)$ of $SrVO_3$, however, suggests that the t_{2g} orbitals are mixed and become split to activate interband transition.

Wannier model calculations show that orbital off-diagonal hoppings between V sites separated at larger than the nearest-neighbor distance are responsible for the band splitting and the interband transition. Figure 3(c) displays the band dispersion from the Wannier model calculations with and without orbital off-diagonal hoppings. The effect of the orbital off-diagonal hopping is most pronounced in the Γ-M direction. When the orbital off-diagonal hoppings are set to zero (red line), two bands are present in the Γ-M direction. We find that the optical conductivity calculated from the band structure without the orbital off-diagonal hoppings displays no interband transitions. When the full Hamiltonian, which includes the orbital off-diagonal hoppings, is employed, the lower energy degenerate band (red line) becomes split into two bands (black line). The energy difference between the split bands is about 0.15 eV, which matches with the peak position of the interband transition in the $\sigma_1(\omega)$ from the DFT calculations [Fig. 3(b)].

To encode the effect of the electron–electron correlations, DMFT calculations were carried out by adding local (*d*-*d*) on-

site interactions of the Hubbard–Kanamori form [59]:

$$H = U\sum_{l} n_{l\uparrow}n_{l\downarrow} + \sum_{l<l',\sigma}[U' n_{l\sigma}n_{l'\bar{\sigma}} + (U'-J)n_{l\sigma}n_{l'\sigma} - J c^{\dagger}_{l\sigma}c_{l\bar{\sigma}}c^{\dagger}_{l'\bar{\sigma}}c_{l'\sigma}] - J\sum_{l<l'}[c^{\dagger}_{l\uparrow}c^{\dagger}_{l\downarrow}c_{l'\uparrow}c_{l'\downarrow} + \text{H.c.}], \quad (1)$$

with $l \in \{xy,\ xz,\ yz\}$ and $U' = U - 2J$, and solving the resulting model within the DFT plus single-site DMFT method [44,46,60]. We used the parameters of $U = 5.0$ eV and $J = 0.6$ eV, which are appropriate values for $SrVO_3$ [28,61]. The momentum-resolved spectral function from the DFT + DMFT calculations (color-coded) in Fig. 3(a) shows an approximate factor of 2 renormalization of the bandwidth. The interband splitting is similarly renormalized. Accordingly, the optical conductivity calculated with the full DMFT self-energy yields the interband transition located at about 0.07 eV [Fig. 3(b)], which agrees well with the peak position of the experimentally observed optical excitation.

Knowing that the majority of the spectral weight at about 0.07 eV comes from the interband transitions, we show that the interband transitions can mimic the non-Fermi-liquid behavior of the charge dynamics. In single-band correlated metals, the memory function analysis was employed to investigate many-body effects on the intraband component of the optical conductivity [17,18,62,63]:

$$\sigma(\omega) = \frac{i\varepsilon_0\omega_p^2}{\omega + M(\omega)}, \quad (2)$$

where ε_0 is the permittivity of free space and ω_p is the plasma frequency. The complex memory function $M(\omega) = M_1(\omega) + iM_2(\omega)$ corresponds to the optical self-energy and reflects the renormalization of the mass and the lifetime of itinerant carriers. They can be calculated from the optical conductivity $\sigma(\omega)$ [17,18,62,63]:

$$1 + \frac{M_1(\omega)}{\omega} = \frac{m^*(\omega)}{m_b} = -\text{Im}\left[\frac{\varepsilon_0\omega_p^2}{\omega\sigma(\omega)}\right] \quad (3)$$

and

$$M_2(\omega) = \frac{1}{\tau(\omega)} = \text{Re}\left[\frac{\varepsilon_0\omega_p^2}{\sigma(\omega)}\right]. \quad (4)$$

Here m_b is the band mass, and $m^*(\omega)$ and $1/\tau(\omega)$ are the frequency-dependent effective mass and scattering rate, respectively. The renormalization of the lifetime and the effective mass of the itinerant carriers leads to the deviation of the optical conductivity from the Drude response where the mass enhancement is one and the scattering rate is constant. For Fermi-liquid quasiparticles, the real and imaginary parts of the memory function are expected to show linear and quadratic frequency dependences, respectively. Deviations from the Fermi-liquid behaviors of the memory function are attributed to electron–boson or electron–electron interactions [5,18].

We display the real and imaginary parts of the memory function of the $SrVO_3$ films calculated directly from the data in Fig. 4. The memory functions of both the SVO-130 and SVO-6 samples share the same spectral trends, but differ in their absolute magnitude. The $M_1(\omega)$ and $M_2(\omega)$ show the linear and the quadratic frequency dependences in the energy region below 50 meV, respectively, as expected for a Fermi liquid. In the higher energy region, a deviation of the $M_1(\omega)$ and the $M_2(\omega)$ from the Fermi-liquid behavior is registered. The $M_1(\omega)$ has a weak maximum at about 60 meV and decreases slightly at higher energies. The $M_2(\omega)$ exhibits a linear frequency dependence at $\hbar\omega > 60$ meV. These behaviors of the memory function are widely observed in various correlated metals, including the doped cuprates, titanates, and the ruthenates, and are linked to non-Fermi-liquid self-energies [5,8,18].

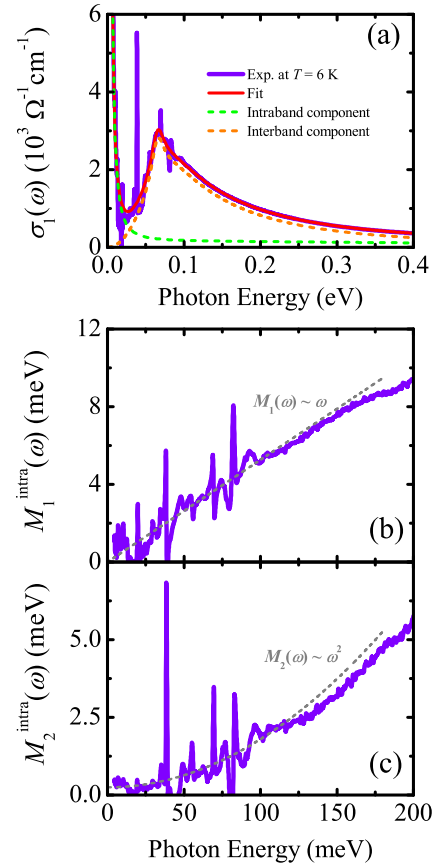

FIG. 5. (a) Drude–Lorentz fitting results of $\sigma_1(\omega)$ of the SVO-130 sample at 6 K. (b) The real part and (c) the imaginary part of the memory function for the intraband response [$M_1^{\text{intra}}(\omega)$ and $M_2^{\text{intra}}(\omega)$] of the SVO-130 sample at 6 K.

We stress that the energies at which the deviation from the Fermi-liquid behavior of the memory function coincide with those where the interband transitions are observed in $\sigma_1(\omega)$. To isolate the memory function corresponding to the intraband response, $M^{\text{intra}}(\omega)$, we fit the $\sigma(\omega)$ by using the Drude–Lorentz model and subtract the interband contributions from the experimental $\sigma(\omega)$. We employ two Drude oscillators for the intraband response and one Lorentz oscillator for the interband transition. The best-fit result for the $\sigma_1(\omega)$ data of the SVO-130 sample is shown in Fig. 5(a). For the $M^{\text{intra}}(\omega)$ shown in Figs. 5(b) and 5(c), the pronounced deviations from the Fermi-liquid behavior at the energies $\hbar\omega \geqslant 50$ meV in the $M(\omega)$ is drastically suppressed, and the Fermi-liquid behavior, i.e., $M_1^{\text{intra}}(\omega) \sim \omega$ and $M_2^{\text{intra}}(\omega) \sim \omega^2$, persists in the energies at least up to 100 meV. This analysis highlights that the non-Fermi-liquid behavior observed in the $M(\omega)$ is mostly due to the interband transitions.

While the DFT + DMFT calculations presented here reproduce the main spectral features of the experimental data, there is a quantitative difference in the magnitude of $\sigma_1(\omega)$ at $\hbar\omega > 70$ meV. The calculated conductivity is substantially smaller than the measured conductivity. This difference may be attributed to effects that are not included in our DMFT calculations, such as electron–phonon interactions and/or vertex corrections. Electron–phonon coupling may give rise to a formation of the sideband in the phonon energy region. While a kink structure, which is attributed to an electron–phonon coupling, in the band dispersion at about 60 meV below the Fermi energy is reported [32], the effects of the electron–phonon coupling to the self-energy is found to be weak [32,64]. Single-band Hubbard model studies show that vertex corrections can affect the optical conductivity in the gap energy region [65–68]. The effects of the vertex corrections may be enhanced in multiband systems, which is the case with $SrVO_3$ [5]. On the other hand, we note that the intraband conductivity extracted from the experimental data [Fig. 5(a)] are quite close to that from the DFT + DMFT calculations [Fig. 3(b)]. This suggests that the origin of the difference between the calculated and measured conductivity may be with understanding the interband transitions. Further studies are required to address this issue.

Our finding of the low-energy interband transition in the $\sigma_1(\omega)$ of SVO demands a revisit of the optical response of the correlated electron system. Due to the cubic symmetry of SVO, the orbital off-diagonal hopping has been expected to be strongly suppressed and to hardly affect the low-energy electronic response. However, our result reveals that the weak orbital off-diagonal hopping between further neighbors can induce strong interband transitions in the energy region where the tail of the Drude-like peak is present. For the samples with a higher degree of disorder, the Drude peak masked this interband transition, resulting in the spectral shape mimicking the non-Fermi-liquid behavior, as exemplified in the SVO-6 sample. Similar phenomena can, in general, happen in any multiband materials. In particular, multiband materials with the $GdFeO_3$-type orthorhombic distortion, such as the perovskite-type titanates, vanadates, and ruthenates, may have stronger low-energy interband transitions than the cubic $SrVO_3$, because the orbital off-diagonal hoppings are allowed not only between the further nearest neighbors, but also between the nearest neighbors in the distorted structure.

IV. CONCLUSIONS

We investigated the electronic response of $SrVO_3$ thin films with different degrees of disorder using infrared spectroscopy and DFT + DMFT calculations. We observed a strong excitation in the optical conductivity at about 70 meV in ultraclean $SrVO_3$. The DFT + DMFT and the Wannier model calculations revealed that the peak should be assigned to interband transitions induced by long-range orbital off-diagonal hoppings between V sites. The memory function analysis showed that interband transition affected the optical self-energy, resulting in a deviation from the expected Fermi-liquid behavior. By properly taking the newly discovered low-energy interband transition into account and correcting the memory function, the Fermi-liquid behavior for ultraclean $SrVO_3$ is found as well. Our studies show that a new material quality of correlated electron systems helps elucidate the role that even minute band structure features can play, which needs to be considered when analyzing the charge dynamics of correlated electron systems.

ACKNOWLEDGEMENTS

This work was supported by a National Research Foundation of Korea grant funded by the Korea government (MSIT) (Grant No. 2022R1F1A1072865) and by the Brain-Link program funded by the Ministry of Science and ICT through the National Research Foundation of Korea (Grant No. 2022H1D3A3A01077468). M.B. and R.E.-H. acknowledge support from the Department of Energy (Grant No. DE-SC0012375). J.D.R. and R.E.-H. acknowledge the National Science Foundation (Grant No. DMR-1629477), and J.D.R. acknowledges support from the NSF Graduate Research Fellowship Program under Grant No. DGE1255832. A.J.M. was supported as part of the Energy Frontier Research Center on Programmable Quantum Materials funded by the U.S. Department of Energy, Office of Science, Basic Energy Sciences, under Award No. DE-SC0019443. The Flatiron Institute is supported by the Simons Foundation. Part of this study has been performed using facilities at the IBS Center for Correlated Electron Systems, Seoul National University.

[1] L. D. Landau, Sov. Phys. JETP **3**, 920 (1957).
[2] P. A. Lee, N. Nagaosa, and X.- G. Wen, Rev. Mod. Phys. **78**, 17 (2006).
[3] C. M. Varma, Rev. Mod. Phys. **92**, 031001 (2020).
[4] R. L. Greene, P. R. Mandal, N. R. Poniatowski, and T. Sarkar, Annu. Rev. Condens. Matter Phys. **11**, 213 (2020).
[5] D. N. Basov, R. D. Averitt, D. van der Marel, M. Dressel, and K. Haule, Rev. Mod. Phys. **83**, 471 (2011).
[6] D. N. Basov and T. Timusk, Rev. Mod. Phys. **77**, 721 (2005).
[7] M. Imada, A. Fujimori, and Y. Tokura, Rev. Mod. Phys. **70**, 1039 (1998).
[8] P. Kostic, Y. Okada, N. C. Collins, Z. Schlesinger, J. W. Reiner, L. Klein, A. Kapitulnik, T. H. Geballe, and M. R. Beasley, Phys. Rev. Lett. **81**, 2498 (1998).
[9] J. S. Dodge, C. P. Weber, J. Corson, J. Orenstein, Z. Schlesinger, J. W. Reiner, and M. R. Beasley, Phys. Rev. Lett. **85**, 4932 (2000).
[10] Y. S. Lee, J. Yu, J. S. Lee, T. W. Noh, T. H. Gimm, H.- Y. Choi, and C. B. Eom, Phys. Rev. B **66**, 041104(R) (2002).
[11] S. Kamal, D. M. Kim, C. B. Eom, and J. S. Dodge, Phys. Rev. B **74**, 165115 (2006).
[12] D. van der Marel, H. J. A. Molegraaf, J. Zaanen, Z. Nussinov, F. Carbone, A. Damascelli, H. Eisaki, M. Greven, P. H. Kes, and M. Li, Nature (London) **425**, 271 (2003).
[13] J. Hwang, T. Timusk, and G. D. Gu, J. Phys. Condens. Matter **19**, 125208 (2007).
[14] X. Deng, J. Mravlje, R. Žitko, M. Ferrero, G. Kotliar, and A. Georges, Phys. Rev. Lett. **110**, 086401 (2013).

[15] W. Xu, K. Haule, and G. Kotliar, Phys. Rev. Lett. **111**, 036401 (2013).

[16] X. Deng, K. Haule, and G. Kotliar, Phys. Rev. Lett. **116**, 256401 (2016).

[17] C. Berthod, J. Mravlje, X. Deng, R. Žitko, D. van der Marel, and A. Georges, Phys. Rev. B **87**, 115109 (2013).

[18] D. Stricker, J. Mravlje, C. Berthod, R. Fittipaldi, A. Vecchione, A. Georges, and D. van der Marel, Phys. Rev. Lett. **113**, 087404 (2014).

[19] X. Deng, A. Sternbach, K. Haule, D. N. Basov, and G. Kotliar, Phys. Rev. Lett. **113**, 246404 (2014).

[20] Y. Liu, H. P. Nair, J. P. Ruf, D. G. Schlom, and K. M. Shen, Phys. Rev. B **98**, 041110(R) (2018).

[21] H. T. Dang, J. Mravlje, A. Georges, and A. J. Millis, Phys. Rev. Lett. **115**, 107003 (2015).

[22] L. J. Sandilands, W. Kyung, S. Y. Kim, J. Son, J. Kwon, T. D. Kang, Y. Yoshida, S. J. Moon, C. Kim, and T. W. Noh, Phys. Rev. Lett. **119**, 267402 (2017).

[23] M. Onoda, H. Ohta, and H. Nagasawa, Solid State Commun. **79**, 281 (1991).

[24] I. H. Inoue, O. Goto, H. Makino, N. E. Hussey, and M. Ishikawa, Phys. Rev. B **58**, 4372 (1998).

[25] H. Makino, I. H. Inoue, M. J. Rozenberg, I. Hase, Y. Aiura, and S. Onari, Phys. Rev. B **58**, 4384 (1998).

[26] M. J. Rey, P. Dehaudt, J. C. Joubert, B. Lambert-Andron, M. Cyrot, and F. Cyrot-Lackmann, J. Solid State Chem. **86**, 101 (1990).

[27] T. Mizokawa and A. Fujimori, Phys. Rev. B **54**, 5368 (1996).

[28] E. Pavarini, S. Biermann, A. Poteryaev, A. I. Lichtenstein, A. Georges, and O. K. Andersen, Phys. Rev. Lett. **92**, 176403 (2004).

[29] Z. Zhong, Q. Zhang, and K. Held, Phys. Rev. B **88**, 125401 (2013).

[30] T. Yoshida, K. Tanaka, H. Yagi, A. Ino, H. Eisaki, A. Fujimori, and Z. X. Shen, Phys. Rev. Lett. **95**, 146404 (2005).

[31] T. Yoshida, M. Hashimoto, T. Takizawa, A. Fujimori, M. Kubota, K. Ono, and H. Eisaki, Phys. Rev. B **82**, 085119 (2010).

[32] S. Aizaki, T. Yoshida, K. Yoshimatsu, M. Takizawa, M. Minohara, S. Ideta, A. Fujimori, K. Gupta, P. Mahadevan, K. Horiba, H. Kumigashira, and M. Oshima, Phys. Rev. Lett. **109**, 056401 (2012).

[33] T. Mitsuhashi, M. Minohara, R. Yukawa, M. Kitamura, K. Horiba, M. Kobayashi, and H. Kumigashira, Phys. Rev. B **94**, 125148 (2016).

[34] M. Brahlek, A. S. Gupta, J. Lapano, J. Roth, H.- T. Zhang, L. Zhang, R. Haislmaier, and R. Engel-Herbert, Adv. Funct. Mater. **28**, 1702772 (2018).

[35] M. Brahlek, L. Zhang, C. Eaton, H.- T. Zhang, and R. Engel-Herbert, Appl. Phys. Lett. **107**, 143108 (2015).

[36] C. C. Homes, M. Reedyk, D. A. Cradles, and T. Timunsk, Appl. Opt. **32**, 2976 (1993).

[37] A. B. Kuzmenko, Rev. Sci. Instrum. **76**, 083108 (2005).

[38] See Supplemental Material at http://link.aps.org/supplemental/10.1103/PhysRevB.106.085133 which includes Refs. [39–41], for the details of the reflectivity measurements, raw reflectivity data, the analyses of the optical data, and the theoretical calculations.

[39] L. J. Sandilands, A. A. Reijnders, A. H. Su, V. Baydina, Z. Xu, A. Yang, G. Gu, T. Pedersen, F. Borondics, and K. S. Burch, Phys. Rev. B **90**, 081402(R) (2014).

[40] A. A. Schafgans, K. W. Post, A. A. Taskin, Y. Ando, X.- L. Qi, B. C. Chapler, and D. N. Basov, Phys. Rev. B **85**, 195440 (2012).

[41] C. Ambrosch-Draxl and J. O. Sofo, Comput. Phys. Commun. **175**, 1 (2006).

[42] P. Blaha, K. Schwarz, K. H. Madsen, D. Kvasnicka, J. Luitz, R. Laskowski, F. Tran, and L. D. Marks, *WIEN2k: An Augmented Plane Wave + Local Orbitals Program for Calculating Crystal Properties* (Vienna University of Technology, Vienna, 2018).

[43] J. P. Perdew, K. Burke, and M. Ernzerhof, Phys. Rev. Lett. **77**, 3865 (1996).

[44] M. Aichhorn, L. Pourovskii, P. Seth, V. Vildosola, M. Zingl, O. E. Peil, X. Deng, J. Mravlje, G. J. Kraberger, C. Martins, M. Ferrero, and O. Parcollet, Comput. Phys. Commun. **204**, 200 (2016).

[45] P. Seth, I. Krivenko, M. Ferrero, and O. Parcollet, Comput. Phys. Commun. **200**, 274 (2016).

[46] O. Parcollet, M. Ferrero, T. Ayral, H. Hafermann, I. Krivenko, L. Messio, and P. Seth, Comput. Phys. Commun. **196**, 398 (2015).

[47] J. Kuneš, R. Arita, P. Wissgott, A. Toschi, H. Ikeda, and K. Held, Comput. Phys. Commun. **181**, 1888 (2010).

[48] A. A. Mostofi, J. R. Yates, Y.- S. Lee, I. Souza, D. Vanderbilt, and N. Marzari, Comput. Phys. Commun. **178**, 685 (2008).

[49] N. Marzari and D. Vanderbilt, Phys. Rev. B **56**, 12847 (1997).

[50] I. Souza, N. Marzari, and D. Vanderbilt, Phys. Rev. B **65**, 035109 (2001).

[51] W. C. Sheets, B. Mercey, and W. Prellier, Appl. Phys. Lett. **91**, 192102 (2007).

[52] H. Koinuma, M. Yoshimoto, H. Nagata, and T. Tsukahara, Solid State Commun. **80**, 9 (1991).

[53] B. L. Chamberland and P. S. Danielson, J. Solid State Chem. **3**, 243 (1971).

[54] M. Gu, S. A. Wolf, and J. Lu, Adv. Mater. Interfaces **1**, 1300126 (2014).

[55] A. Fouchet, M. Allain, B. Bérini, E. Popova, P.- E. Janolin, N. Guiblin, E. Chikoidze, J. Scola, D. Hrabovsky, Y. Dumont, and N. Keller, Mater. Sci. Eng. B **212**, 7 (2016).

[56] M. Takizawa, M. Minohara, H. Kumigashira, D. Toyota, D. Oshima, H. Wadati, T. Yoshida, A. Fujimori, M. Lippmaa, M. Kawasaki, H. Koinuma, G. Sordi, and M. Rozenberg, Phys. Rev. B **80**, 235104 (2009).

[57] R. Sakuma, P. Werner, and F. Aryasetiawan, Phys. Rev. B **88**, 235110 (2013).

[58] I. A. Nekrasov, K. Held, G. Keller, D. E. Kondakov, T. Pruschke, M. Kollar, O. K. Andersen, V. I. Anisimov, and D. Vollhardt, Phys. Rev. B **73**, 155112 (2006).

[59] J. Kanamori, Prog. Theor. Exp. Phys. **30**, 275 (1963).

[60] A. Georges, G. Kotliar, W. Krauth, and M. J. Rozenberg, Rev. Mod. Phys. **68**, 13 (1996).

[61] K. Held, G. Keller, V. Eyert, D. Vollhardt, and V. I. Anisimov, Phys. Rev. Lett. **86**, 5345 (2001).

[62] W. Götze and P. Wölfle, Phys. Rev. B **6**, 1226 (1972).

[63] A. V. Puchkov, D. N. Basov, and T. Timusk, J. Phys. Condens. Matter **8**, 10049 (1996).

[64] M. Kobayashi, K. Yoshimatsu, E. Sakai, M. Kitamura, K. Horiba, A. Fujimori, and H. Kumigashira, Phys. Rev. Lett. **115**, 076801 (2015).

[65] N. Lin, E. Gull, and A. J. Millis, Phys. Rev. B **80**, 161105(R) (2009).

[66] J. Vučičević, J. Kokalj, R. Žitko, N. Wentzell, D. Tanasković, and J. Mravlje, Phys. Rev. Lett. **123**, 036601 (2019).

[67] A. Kauch, P. Pudleiner, K. Astleithner, P. Thunström, T. Ribic, and K. Held, Phys. Rev. Lett. **124**, 047401 (2020).

[68] D. N. Aristov and R. Zeyher, Phys. Rev. B **72**, 115118 (2005).